



## ESTIMATION OF THE DURATIONS OF BREAKS IN DEPOSITION – SPELEOTHEM CASE STUDY

J. PAWLAK<sup>1</sup>\*, H. HERCMAN<sup>1</sup>, P. SIERPIEŃ<sup>1</sup>, P. PRUNER<sup>2,3</sup>, M. GAŚSIOROWSKI<sup>1</sup>, A. MIHEVC<sup>3</sup>, N. ZUPAN HAJNA<sup>3</sup>, P. BOSÁK<sup>2,3</sup>, M. BŁASZCZYK<sup>1</sup>, B. WACH<sup>1</sup>

<sup>1</sup>Institute of Geological Sciences of the Polish Academy of Sciences, Twarda 51/55, 00-818 Warszawa, Poland

<sup>2</sup>Institute of Geology of the Czech Academy of Sciences, Rozvojová 269, 165 00 Praha 6, Czech Republic

<sup>3</sup>ZRC SAZU Karst Research Institute, Titov trg 2, 6230 Postojna, Slovenia

Received 07 October 2019

Accepted 28 August 2020

### Abstract

Speleothems provide one of the most continuous terrestrial archives. However, due to changing conditions in temperature/humidity or the chemistry of percolating water, sedimentation breaks (hiatuses) and erosional events are possible and are commonly recorded in speleothems. Sedimentation breaks with durations longer than the resolution of the studied record should be considered in potential speleothem age-depth models. The most classic and reliable solution to the problem is the independent construction of age-depth models for the parts of speleothems separated by the hiatuses. However, in some cases, it is not possible to obtain a sufficient number of dating results for reliable age-depth model estimation. In such cases, the problem can be solved by the application of other sources of chronological information. Here, based on a few speleothem examples, an alternative approach – oxygen isotopic stratigraphy – is used to estimate the chronology for the parts of speleothems where there is not enough chronological information for classic age-depth models. As a result, the deposition break duration can be estimated.

### Keywords

age-depth models; oxygen isotope stratigraphy; paleomagnetism; U-series dating.

## 1. Introduction

Speleothems are valuable archives of paleoenvironmental information. Their isotopic compositions of O and C and trace element contents, e.g., Mg, Sr, and Ba, are valuable sources of data on local conditions, such as the amount of precipitation or mean air temperature (Baker *et al.*, 1993; Frisia *et al.*, 2003; Roberts *et al.*, 1998; Hu *et al.*, 2008; Yuan *et al.*, 2004; Wang *et al.*, 2001, 2005; Fairchild and Baker, 2012). The additional advantage of speleothems is the fact that their age can be precisely estimated by the U-series method (Ivanovich and Harmon, 1992; Fairchild and Baker, 2012). Speleothem archives cover long periods of time and are usually one of the most continuous terrestrial archives. However, due to changing deposition conditions (e.g., temperature/humidity) or percolating water

chemistry, breaks (hiatuses) in speleothem crystallization and erosional events are possible and relatively common (Fairchild and Baker, 2012).

According to Sadler (1981), sedimentation is essentially a discontinuous process. This is also true in the case of speleothems. Speleothems growth depend on specific conditions, such as the availability of water and its chemical composition, temperature, and CO<sub>2</sub> pressure in the cave atmosphere, which must be lower than that in the dripping water so the degassing process can occur (Fairchild and Baker, 2012). In many cases, those requirements for speleothems crystallization are fulfilled only during the wet and/or warm season of the year. Therefore, speleothems deposition occurs seasonally (Banner *et al.*, 2007). However, seasonal sedimentation breaks are usually not detectable, and their duration is shorter than the resolution of the potential

Corresponding author: Jacek Pawlak  
e-mail: [dzeq@twarda.pan.pl](mailto:dzeq@twarda.pan.pl)

paleoenvironmental records. Sedimentation breaks with durations longer than the resolution of the studied record (hiatuses) are an important problem in age-depth model construction, but they are themselves a source of additional and valuable climatic information. Their occurrence can relate to environmental changes such as turning into colder/dryer climates or very local conditions such as changes in seepage water systems. The potential missing time hidden inside the hiatus is not only the duration of the potential break in sedimentation but also the time connected with potentially eroded strata.

The estimated age scale (chronology) for speleothems should consider the occurrence of the hiatuses. The most classic way to do that, commonly used in published works, is the dating of speleothem layers just below and above the hiatus visible in macro- or microscopic images and the calculation of the duration of the missing part of the profile based on the time difference between those two ages (Fankhauser *et al.*, 2016; Steponaitis *et al.*, 2015). However, this approach does not consider the fact that the sampled points are usually not placed directly on the hiatus borders. Therefore, the estimated hiatus duration includes, in addition to the deposition break duration and the part of the potentially eroded record, time recorded in the part of the profile between the dated points and hiatus. The more reliable solution is independent construction of age-depth models for parts of speleothems separated by hiatuses and the hiatus duration estimation based on the modeled ages of the hiatus borders (Lauritzen, 1995; Holzkamper *et al.*, 2005; Vaks *et al.*, 2006; Spötl and Mangini, 2007; Couchoud *et al.*, 2009; Vansteenberghe *et al.*, 2016). This solution requires several reliable dating results or other time benchmarks for every continuous deposition phase. In some cases, such as a small thickness of the deposition phase or low quality of the speleothem material (e.g., high contamination by thorium (Th) and uranium (U) from the noncarbonate fraction or high porosity), it is not possible to obtain enough dating results for reliable age-depth model estimation (Jo *et al.*, 2011). In such situations, the classic age-depth model approach cannot be used, and part of the stalagmite is left without precise chronology (see Jo *et al.*, 2011). However, the problem can be solved by using other potential sources of chronological information.

Here, we present several examples of speleothem records with clearly visible hiatuses and possible methods of estimating the durations of the hiatuses. The first and the simplest example is the PD-4 stalagmite (Demänovská Cave System, Slovakia), where the hiatus duration can be estimated based on the classic age-depth modeling approach. The second example, the SC-3 stalagmite (Szczelina Chochołowska Cave, Tatra Mts., Poland), represents the situation where the alternative approach - oxygen isotopic stratigraphy (OIS) - is used to obtain additional

chronological information for the part of the stalagmite located between hiatuses and where only one U-series age is available. Finally, the OIS and age-depth modeling approaches were tested on previously published data from Spain, Macedonia and South Korea. The last example is the flowstone profile in Ledena Dvorana (LDH; Snežna Cave, Slovenia). The LDH profile is divided by ten principal hiatuses. Its chronology is based on a set of paleomagnetic benchmarks. However, their number is too low for the estimation of age-depth models for every deposition phase by classic age-depth modeling. This profile is an example of how the chronology of the whole profile can be estimated based on OIS and independent age benchmarks.

## 2. Material and Local Settings

### 2.1 PD-4 stalagmite

The PD-4 stalagmite was collected in the Demänovský jaskynný systém (Demänová Cave System, DCS). The DCS is situated in the Nízke Tatry (Low Tatra) Mountains (Western Carpathians, Slovakia; 19.58° E 49° N; the entrance elevation is 812 and 837 m.a.s.l; Fig. 1A). The total length of the DCS corridors is approximately 41.4 km (Herich, 2017). The PD-4 sample was taken in the Pekelný Dóm Chamber, located at the lower level of the DCS with the active underground stream of the Demänovka Stream. PD-4 is an approximately 385-mm-long calcite stalagmite of light cream color. The stalagmite is divided into two parts by a layer of sand cemented by calcite. This layer documents the break in calcite crystallization and filling of the cave passage by sand. The part of the stalagmite below the sand layer is 96 mm long. The calcite here is laminated and has several macroscopically visible pores. These pores do not contain any detrital particles or younger crystallization traces. The part of the stalagmite above the sand layer is 290 mm long, and it has lamination, color and porosity similar to that of the lower part (Fig. 1C).

### 2.2 SC-3 stalagmite

The SC-3 stalagmite has been collected in Szczelina Chochołowska Cave in Tatra Mts (Błaszczuk *et al.*, 2020). The SC-3 stalagmite is approximately 240 mm long and contains four phases of continuous growth separated by three discontinuities. These growth interruptions are underlined with layers of detrital material (Fig. 1D) and was identified at 186 mm (H-1), 196.6 mm (H-2) and 230 mm (H-3) from the base of the stalagmite (Błaszczuk *et al.*, 2020).

### 2.3 Ledena Dvorana flowstone profile

Snežna Jama (Ice Cave) is located on the southeastern slope of Raduha Mountain in the northeastern part of the Kam-

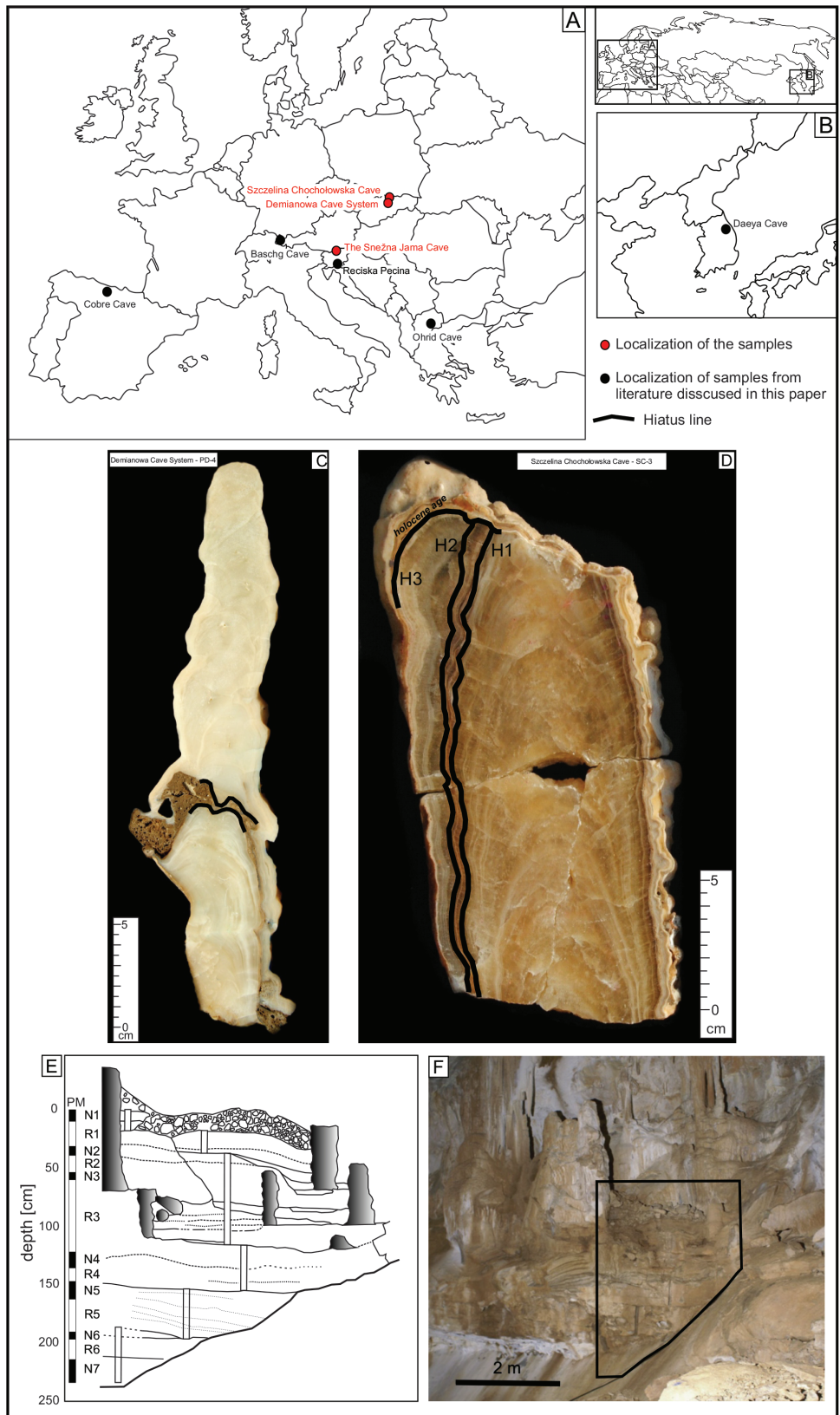


**Fig 1.** Sample localization: A – map of Central Europe; B – map of Korea; C – PD-4 stalagmite (photo by J. Pawlak); D – SC-3 stalagmite (photo by J. Pawlak); E – sketch of the LDH profile with sampled sections (rectangles) and principal hiatuses (lines); F – LDH flowstone.

nik–Savinja Alps (Kamniško–Savinjske Alpe, NW Slovenia, 46°23'53"N, 14°44'31"E, 1514 m.a.s.l.; Fig. 1A). The speleothem profile is situated in the Ledena Dvorana (Ice Hall – LDH), approximately 90 m from the cave entrance at a depth of approximately 45 m below the entrance. The speleothems were deposited as an approximately 2.4-m-thick complex sequence of flowstone (Fig. 1F). Numerous breaks in deposition (hiatuses) are expressed as more or less distinct horizontal, inclined or wavy bedding plains of different character and strength. Hierarchically, the most important breaks in the deposition of flowstones are characterized by the growth of stalagmites, corrosion surfaces, fissuration (e.g., 160 and 700 mm), and by the pseudo-oolithic bases of some overlying layers (e.g., 720 mm). Less important hiatuses are mostly expressed as single bedding plain unconformities. The stalagmites grew during several different periods, especially in the upper half of the profile (above approximately 155 cm). They were completely buried by younger sequences of flowstone. Some of them were broken off approximately at the level of the next distinct hiatus. Judging from their length (mostly up to 500 mm; Bosák *et al.*, 2002), it is believed that their growth required only a few tens of ka. The LDH profile drawing and scheme of unconformities (Bosák *et al.*, 2002; Zupan Hajna *et al.*, 2008; Häuselmann *et al.*, 2015) were originally correlated with speleothem slabs cut from the profile and used for stable isotope study.

The high-resolution paleomagnetic (PM) analysis (Bosák *et al.*, 2002) identified a complex magnetostratigraphic profile (Fig. 1E) with an alternation of seven normal (N)-polarized and six reverse (R)-polarized magnetozones. Detailed paleomagnetic study of the profile shows some magnetozones borders (at 163.7 or 1530 mm) are located at the deposition breaks (in Table 2 marked as italic). Obtained magnetozones scheme was correlated with the GPTS (Ogg, 2012) and was interpreted successively by Bosák *et al.*, (2002), Zupan Hajna *et al.*, (2008), and finally by Häuselmann *et al.*, (2015). Authors stressed the correlation problems caused by partial erosion of the flowstone sequence. The succession, boundary depths and ages of the magnetozones are summarized in Table 2. The magnetozones are numbered from the top to the base. Their boundaries (PM benchmarks) are marked by numbered N/R or R/N symbols. Each benchmark is characterized by two parameters: (a) the depth with errors resulting from the field measurements (using wooden or tape measures) and (b) boundary ages (according to Ogg, 2012) with assumed uncertainty of 1.5%.

U-series analyses of several samples collected from the profile prove the age of flowstone sequence is out of U-Th method range. The previous measurements of uranium concentration in the set of samples from the LDH profile gave results in the range from 0.02 ppm to 0.07 ppm

(Häuselmann *et al.*, 2015), far too low for applying uranium–lead chronology.

### 3. Methods

#### 3.1 U-series dating

Calcite samples were drilled along the profiles of the studied speleothems. The mass of the collected samples was in the range of 0.1–0.5 g. The thicknesses of the sampled layers were up to 2–4 mm. Chemical treatment was performed at the U-series Laboratory of the Institute of Geological Sciences, Polish Academy of Sciences (Warsaw, Poland). First, the samples were treated at high temperature (800°C, over 6 h) for decomposition of the organic matter. The isotopic spike ( $^{233}\text{U}$ ,  $^{236}\text{U}$ ,  $^{229}\text{Th}$ ) was added to the samples before the chemical procedure. The samples were dissolved in nitric acid, and uranium and thorium were separated from the carbonate matrix by the chromatographic method using TRU Resin (Hellstrom, 2003). Internal standards and blank samples were treated by the same procedure as that of all the studied samples. The measurements of U and Th isotopic compositions of all samples and standards were performed at the Institute of Geology of the Czech Academy of Sciences (Prague, Czech Republic) by a double-focusing sector-field ICP mass analyzer (Element 2, Thermo Finnigan MAT). The instrument was set on a low mass resolution ( $m/\Delta m \geq 300$ ).

The measurements were corrected for background counts and chemical blanks and reported as the activity ratios. U-series ages were calculated based on measured  $^{230}\text{Th}/^{234}\text{U}$  and  $^{234}\text{U}/^{238}\text{U}$  activity ratios using the newest decay constants (in  $\text{yr}^{-1}$ ):  $\lambda_{238} = (1.55125 \pm 0.0017) \cdot 10^{-10}$  (Jaffey *et al.*, 1971),  $\lambda_{234} = (2.826 \pm 0.0056) \cdot 10^{-6}$  (Cheng *et al.*, 2013),  $\lambda_{232} = (4.95 \pm 0.035) \cdot 10^{-11}$  (Holden, 1990), and  $\lambda_{230} = (9.1577 \pm 0.028) \cdot 10^{-6}$  (Cheng *et al.*, 2013). The age errors were calculated by considering all uncertainties, except the decay constant, using error propagation rules.

#### 3.2 Oxygen isotope analyses

Samples for  $\delta^{18}\text{O}$  analyses were taken along the growth axes of the speleothems by drilling. The analyses were carried out at the Stable Isotope Laboratory, Institute of Geological Sciences, Polish Academy of Sciences, Warsaw. Oxygen stable isotopic composition was determined using a Thermo KIEL IV Carbonate Device coupled with the Finnigan Delta Plus IRMS spectrometer in a dual inlet system. The  $\text{CO}_2$  from the calcite was extracted using orthophosphoric acid (density  $1.94 \text{ g}\cdot\text{dm}^{-3}$ ) at 70°C. International standard NBS 19 was analyzed with every ten samples. The isotope ratios obtained are reported as delta ( $\delta$ ) values and expressed relative to the V-PDB standard. The measurement precision (1 standard deviation) is 0.10‰ for  $\delta^{18}\text{O}$ .

### 3.3 Age-depth model construction

Based on the obtained U-series dating results, an age-depth model was created using the MOD-AGE algorithm (Hercman and Pawlak, 2012). First, the ages included in the model were calculated based on the corrected values of activity ratios. The depth values were described as normal distributions. Age-depth relationships were estimated using the locally weighted scatterplot smoothing (LOESS) technique (Cleveland, 1979). The chosen span value for the LOESS model was the highest value of span, which allowed the estimation of an age-depth model corresponding to all data points inside the  $2\sigma$  error band (Hercman and Pawlak, 2012).

### 3.4 Oxygen isotope stratigraphy

Oxygen isotopic stratigraphy (OIS) is based on the assumption that changes in the  $\delta^{18}\text{O}$  of speleothems have a regional or global nature. Therefore, it is possible to correlate the  $\delta^{18}\text{O}$  record with the reference (global or regional)  $\delta^{18}\text{O}$  record. The potential reference record should have a well-established age scale and high resolution, and it should record environmental changes similar to those of the correlated record. This means that oxygen isotopic composition changes recorded in the studied speleothem record and reference curve should be coincident and controlled by the same factors. Therefore, the correlation should provide additional chronological information. The choice of the proper reference record is crucial here. Long-term marine records or ice core records can be useful as reference records due to their overall regional nature and well-defined time scale (Lisiecki and Raymo, 2005). The speleothem oxygen stable isotope ( $\delta^{18}\text{O}$ ) records require data standardization before correlation with the marine record. Records from different environments may have different amplitudes and mean values. The correlation process uses relative changes in the isotope composition, not absolute values. The  $\delta^{18}\text{O}$  records from different regions and the archives of different types may express the same climate changes but with different amplitudes and mean values. To avoid the potential threats of amplitude differences, the oxygen isotopic records were normalized. We used the same time window to determine the normalized values for the correlated and reference records. There was one mean value determined for all parts separated by hiatuses in the  $\delta^{18}\text{O}$  record from the selected speleothem.

The next problem is the different reactions of caves and oceans to global changes induced by the same factors. During glaciations, for instance, ocean water becomes enriched in heavier oxygen isotopes, while meteoric water is enriched in light oxygen isotopes. For the speleothem records, the  $\delta^{18}\text{O}$  composition of meteoric water is one of the dominant factors. Therefore, we can expect that signals

in the speleothem records will have a negative correlation with the marine signals. To solve this problem, in the case of correlation with marine records, we inverted our speleothem  $\delta^{18}\text{O}$  records for intercorrelation purposes.

The correlation was performed with GenCorr software (Pawlak and Hercman, 2016). GenCorr seeks an optimal correlation (greatest similarity) between two or more isotopic records by using several correlation procedures. The basic procedure assumes no knowledge of the ages of the record and thus attempts their correlation in a completely free mode. The next step requires some knowledge of the likely ages and uses it in correlation. Age information in the form of age-depth models can be put into GenCorr, allowing the procedure to find the optimal fit for two or more records within the limits of the model confidence bands. However, it is not always possible to make continuous age-depth models for every profile. In the most typical situation, only some information about the correlated age records is available, such as a few dating results or knowledge of the likely age limits/boundaries. This type of information may be used for chronological benchmarks in the correlation process. Two types of benchmarks are possible: (i) fixed benchmarks where there is no information about their age uncertainty, and (ii) age information having normal, uniform or skewed distribution (e.g., dating results). The age assigned for a fixed benchmark remains constant during the entire correlation procedure, while ages assigned for nonfixed benchmarks may change according to their distribution. In both cases, the ages assigned for the points between the benchmarks are calculated in a random way. The only assumption here is that the ages assigned for points between the benchmarks have to be in accordance with the ages assigned for the benchmarks and their stratigraphic positions.

The GenCorr correlation was run with a population of 9,000 individual solutions. Each solution represents one possible position for a matched record on a basic reference time scale. The mean Euclidean distance between the records was used as a heuristic function for the genetic algorithm. The procedure was terminated after 320 algorithm cycles, when further improvements in the optimization became insignificant in scale (Pawlak and Hercman, 2016).

The confidence band estimated for the correlation results considers the uncertainty of the reference curve and the alignment uncertainty. At the initial stage of the population creation, a Monte Carlo method is used to randomize the age of the points from the reference curve. Those points are randomized from a normal distribution, which describes their uncertainty, in the range of  $2\sigma$ . In the next step, different individuals, of correlated record, are aligned to different individuals of reference curve. Finally, based on the population of results a confidence band for the correlation results can be estimated and it includes reference curve error and alignment error.

The reference records used for OIS correlation in described examples are the marine stack records and Greenland ice core records. Their chronology was built based on independent age benchmarks and orbital tuning of  $\delta^{18}\text{O}$  records (Lisicki and Raymo 2005). For the purpose of the correlation procedure, we assumed 2.5% error for the used reference records (Lisicki and Raymo 2005). The error of the whole correlation procedure result was estimated based on the Monte Carlo method, taking into account the reference and studied record errors, chronology benchmark errors and the correlation procedure error. The whole correlation procedure was repeated 40 times for every presented example. On the basis of the obtained set of results, the median (age-depth model) and its  $2\sigma$  error were estimated (Pawlak and Hercman, 2016).

### 3.5 Paleomagnetism

Paleomagnetic analyses were completed in the Department of Palaeomagnetism, Institute of Geology of the Czech Academy of Sciences, Průhonice (Czech Republic). Samples were demagnetized by alternating field (AF) and/or demagnetized thermally (TD). The AF demagnetization was carried out up to a field of 100 mT in 12–16 steps. A MAVACS apparatus (Přihoda *et al.*, 1989) was used for the TD. The natural remnant magnetization (NRM) was measured with a JR–6A spinner magnetometer (Jelínek, 1966) and/or a 2G superconducting rock magnetometer with an incorporated AF unit. The magnetic susceptibility (MS) values were measured on KLY–2 (or KLY–3) kappa bridges and a KLF–4A automatic magnetic susceptibility meter (Jelínek, 1966, Jelínek, 1973). The multicomponent analysis technique of Kirschvink (1980) was applied to separate individual NRM components. The characteristic component (high field and/or high temperature) is stable and can be isolated in the AF and/or TD (approximately 15–80 mT, 350–540°C). Fisher statistics (1953) were employed for the calculation of the mean directions of the NRM components derived by the multicomponent analysis. The flowstones are characterized by very low to high NRM and MS values. The NRM intensities are between 0.2 and 523 mA·m<sup>-1</sup>, and the MS values are between -13 and 324 SI units. Applied PM methods, data interpretation and correlations were presented by Zupan Hajna *et al.*, (2008), and a summary and synthesis of the results were presented by Häuselmann *et al.*, (2015).

## 4 Results

### 4.1 Classic approach U-series dating and age-depth modeling (PD-4 stalagmite)

The results of U-series dating of the PD-4 stalagmite are presented in Table 1. The reported errors represent 2 standard deviations. Based on U-series ages, two age-depth

models for continuously deposited parts of the stalagmite have been constructed. The model for the older part was calculated based on 11 U-series ages (Fig. 2). According to the model, stalagmite growth started at  $48^{+1.2}_{-1}$  ka, and the cessation of its growth was at  $32^{+3.2}_{-8.5}$  ka. The model for the part of the stalagmite younger than the sand layer was estimated based on 8 U-series ages (Fig. 2). It shows that calcite crystallization started again at  $16.4^{+0.7}_{-0.6}$  ka and has continued until the present time. Based on the two ages, the age of the cessation in growth of the older stalagmite part and the age of the start of crystallization for the younger part, it is possible to estimate the duration of the sedimentation break. Taking into account the stratigraphic order, the duration of the deposition break could be estimated as  $15.8^{+5.6}_{-9.2}$  ka. The additional U-series age is taken from the thin calcite layer (Fig. 1C) inside the sand, and this age is  $19\pm 0.2$  ka (Fig. 2). The layer records short calcite crystallization phases in the period of cave flooding and sand deposition, indicating a bimodal character of sand deposition.

### 4.2 U-series and age-depth modeling combined with oxygen isotope stratigraphy (SC-3 stalagmite)

A series of fifteen U-series ages were obtained from the whole stalagmite (Błaszczuk *et al.* 2020). In our study, we have used only dates located close to H1 and H2 hiatuses (Table 1). The reported errors represent 2 standard deviations. Only one U-series data point,  $273\pm 5$  ka, was obtained for the layer between the hiatuses (H2 and H1 on Fig. 3). Based on one U-series age, it is not possible to estimate the age-depth model for this part of the stalagmite. The older and younger parts of the studied stalagmite have well-defined age-depth models estimated by MOD-AGE software. The age range of this deposition phases is  $327\pm 7$  ka and  $289\pm 4$  ka for the older phase and  $250^{+10}_{-7}$  to  $200^{+20}_{-17}$  ka for the younger phase.

For the part of the stalagmite between hiatuses, an age-depth relation was constructed using the OIS approach using the LR04 combined record (Lisiecki and Raymo, 2005) as a reference curve. The set of fifteen samples for  $\delta^{18}\text{O}$  analyses was collected from this part of the stalagmite located between the H1 and H2 hiatuses (188–196.5 mm; Fig. 4A) at a resolution of one sample per 0.5 mm. The value of  $\delta^{18}\text{O}$  varies in the range of 1.8‰ (from -7.8‰ to -6‰). Three age benchmarks have been used. The first is the U-series dating result obtained for this part of the stalagmite (Table 1) as an independent age benchmark with a normal distribution. The other two benchmarks are border ages from age-depth models of the parts below the H1 hiatus and above the H2 hiatus. The OIS (Fig. 4B) places the deposition of the stalagmite parts located between the hiatuses in the age range between  $282^{+1}_{-3}$  and  $263^{+2.5}_{-1}$  ka (Fig. 3). The  $\delta^{18}\text{O}$  record has been correlated with the LR04 record using GenCorr software (Pawlak and Hercman, 2016).

**Table 1.** U-series dating results for the SC-3 and PD-4 stalagmites.

sample	H [mm]	U [ppm]	<sup>234</sup> U/ <sup>238</sup> U AR	<sup>230</sup> Th/ <sup>234</sup> U AR	<sup>230</sup> Th/ <sup>232</sup> Th AR	Age [ka]
SC-5	182±1	1.038 ± 0.002	1.158 ± 0.002	0.970 ± 0.005	7842 ± 46	290 ± 7
SC-6	192±1	0.610 ± 0.002	1.105 ± 0.002	0.944 ± 0.004	45 ± 0.2	273 ± 5
SC-8	198.5±1	1.000 ± 0.006	1.158 ± 0.002	0.936 ± 0.005	3345 ± 21	254 ± 5
SC-9	200±1	0.941 ± 0.002	1.100 ± 0.002	0.915 ± 0.008	9078 ± 90	242 ± 7
PD4-1	4±1	1.659 ± 0.003	1.143 ± 0.001	0.351 ± 0.001	374 ± 2	46.6 ± 0.2
PD4-2	12.5±1	2.000 ± 0.01	1.197 ± 0.003	0.334 ± 0.002	654 ± 4	43.8 ± 0.3
PD4-3	23±1	3.335 ± 0.006	1.182 ± 0.003	0.322 ± 0.002	2401 ± 18	41.9 ± 0.3
PD4-4	38±1	2.578 ± 0.004	1.161 ± 0.001	0.320 ± 0.001	2254 ± 8	41.7 ± 0.2
PD4-5	40±1	2.330 ± 0.01	1.185 ± 0.003	0.314 ± 0.002	2960 ± 17	40.7 ± 0.3
PD4-6	50±1	1.840 ± 0.01	1.179 ± 0.003	0.311 ± 0.005	832 ± 13	40.1 ± 0.7
PD4-7	58±1	3.540 ± 0.007	1.152 ± 0.001	0.305 ± 0.001	781 ± 3	39.3 ± 0.1
PD4-8	73±1	2.111 ± 0.004	1.149 ± 0.002	0.295 ± 0.002	2352 ± 19	37.9 ± 0.3
PD4-9	86±1	3.700 ± 0.020	1.142 ± 0.001	0.297 ± 0.001	210 ± 1	37.8 ± 0.3
PD4-10	88±1	2.320 ± 0.004	1.160 ± 0.002	0.282 ± 0.002	220 ± 2	35.8 ± 0.2
PD4-11	90±1	2.318 ± 0.010	1.203 ± 0.004	0.277 ± 0.005	1043 ± 17	35 ± 0.7
PD4-12	107±1	0.751 ± 0.005	1.269 ± 0.007	0.133 ± 0.003	81 ± 2	15.5 ± 0.4
PD4-13	129±1	1.479 ± 0.009	1.219 ± 0.004	0.103 ± 0.002	671 ± 15	11.9 ± 0.3
PD4-14	154±1	1.183 ± 0.007	1.215 ± 0.004	0.082 ± 0.001	338 ± 4	9.4 ± 0.2
PD4-15	183±1	1.386 ± 0.008	1.235 ± 0.003	0.084 ± 0.001	332 ± 6	9.3 ± 0.2
PD4-16	224±1	1.243 ± 0.007	1.242 ± 0.002	0.056 ± 0.001	585 ± 14	6.3 ± 0.2
PD4-17	291±1	1.467 ± 0.009	1.249 ± 0.002	0.055 ± 0.001	667 ± 13	6.2 ± 0.2
PD4-18	364±1	1.469 ± 0.008	1.277 ± 0.003	0.049 ± 0.001	293 ± 6	5.4 ± 0.1
PD4-19	377±1	2.088 ± 0.013	1.302 ± 0.007	0.023 ± 0.001	115 ± 6	2.5 ± 0.1

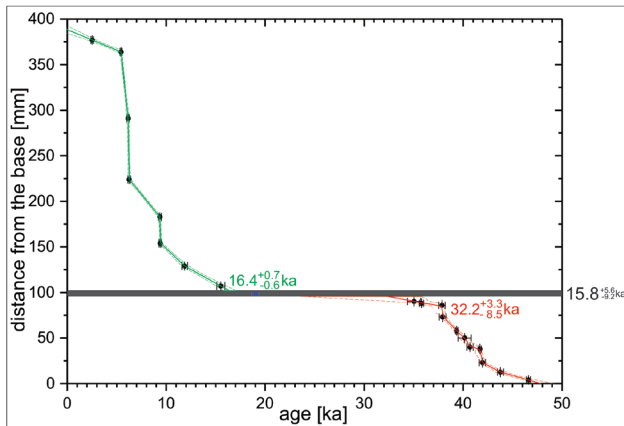


**Fig 2.** Age-depth models for the PD-4 stalagmite with estimated hiatus duration.

Based on the three independent age-depth models, it is possible to estimate the time duration of the H1 and H2 hiatuses. The H1 hiatus covers the time between 289±4 and 282±1 ka, and its duration could be estimated as 7±6 ka. The H2 hiatus covers a longer time period between 263±2.5 and 250±10 ka, and its duration was estimated as 13.5±11 ka (Fig. 3).

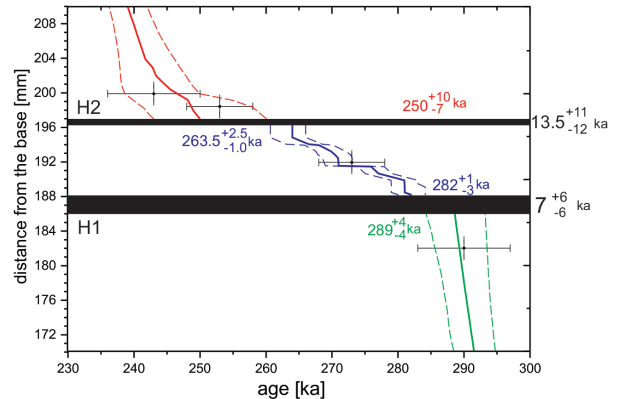


**Fig 3.** Age-depth models for the SC-3 stalagmite with the estimated durations of the hiatuses H1 and H2: A – the age-depth model chart of the whole profile; B – enlarged H1 and H2 zones; age-depth model for the oldest deposition phase (green lines); age-depth model for the deposition phase between H1 and H2 (blue lines); and age-depth model for the youngest deposition phase (red lines).

**4.3 Paleomagnetism (PM) combined with oxygen isotope stratigraphy (OIS) – (Ledena Dvorana – LDH profile).**

The LDH δ<sup>18</sup>O record in its depth scale is presented in Fig. 5A. The δ<sup>18</sup>O values vary from -9.5‰ to almost

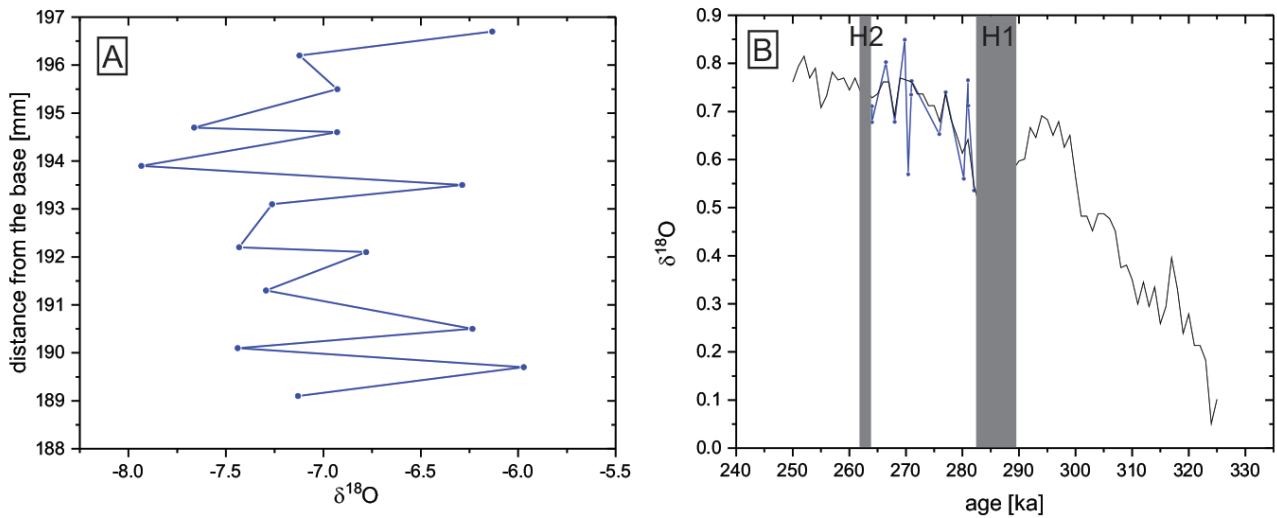


Fig 4. The  $\delta^{18}\text{O}$  data for the SC-3 profile: A – the  $\delta^{18}\text{O}$  record in the depth scale; B – the result of the correlation with the LR04 record.

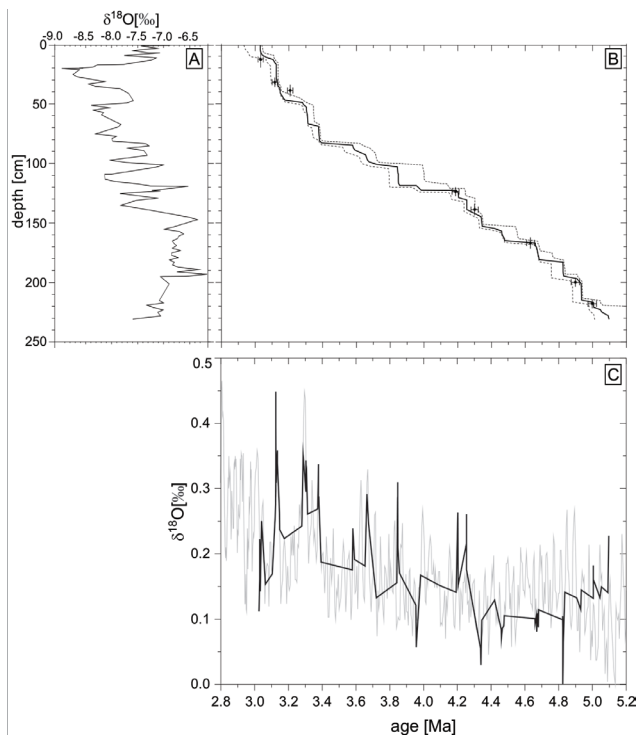


Fig 5. The results of OIS for the LDH profile: A – the  $\delta^{18}\text{O}$  record of the LDH profile in a depth scale; B – age-depth models estimated based on the OIS and the PM approaches (black lines); C – the  $\delta^{18}\text{O}$  record of LDH placed in both age scales and compared with the LR04 record (gray line).

-6.5‰. The record has a clearly visible depleting trend from the 200-cm mark (bottom of the profile) to the top 20 cm. The youngest 20 cm of the record is characterized by a rapid increase from -9.5‰ to -7.5‰  $\delta^{18}\text{O}$ . Apart from these trends, the record contains thirteen cyclic changes with amplitudes of approximately 1‰. The LDH section

contains several visible breaks in deposition, seen as thick lines in Fig. 6. Three of the magnetozones must be located at the hiatuses. It must be assumed that part of those magnetozones must be not deposited or eroded. These age benchmarks (magnetozones boundaries) cannot be used for chronology construction and duration estimation of deposition breaks. Therefore, for the purpose of chronology construction, we use only those PM benchmarks that are located inside the episodes of continuous deposition phases.

The combination of the PM information and the OIS approach (OIS+PM) allows GenCorr (Pawlak and Hercman, 2016) to search for optimal positions within the time intervals defined by the PM benchmarks (Fig. 5C; black line). The OIS+PM correlation places the LDH profile between 2.95 and 5.1 Ma (Fig. 5C; black line). With this solution, the LDH  $\delta^{18}\text{O}$  record is in good agreement with the principal trend in the LR04  $\delta^{18}\text{O}$  record, and the major peaks in the two records are also well correlated (Fig. 5C; black line).

The OIS+PM age-depth model suggests nine hiatuses (Fig. 6B). These hiatuses are in good agreement with the principal hiatuses observed in the LDH profile (Fig. 6A; thick lines). The gray rectangles in Fig. 6B show the suggested duration of those hiatuses.

## 5. Discussion

The estimation of hiatus duration is a common geological problem. In fact, based on the chronological information only, it is not possible to estimate the hiatus duration, which is understood as a non-deposition time. The calculated time is rather a sum of “non-deposition time” plus the time recorded in potentially eroded strata. The time missed in the hiatus can be estimated by the calculation

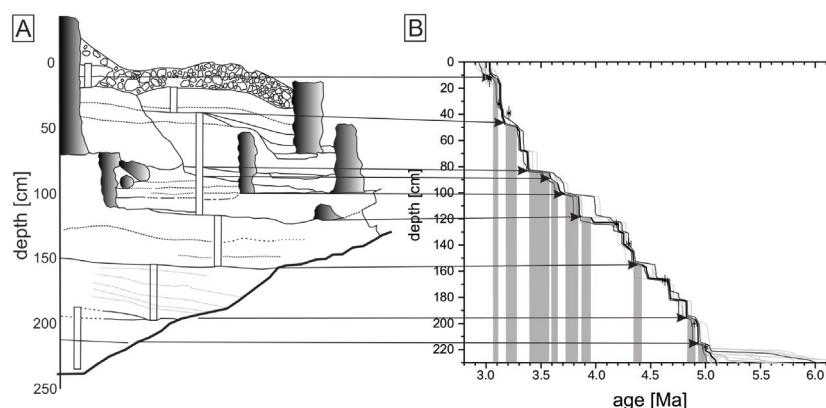


**Fig 6.** LDH profile: A – sketch of the LDH profile with sampled sections (rectangles) and principal hiatuses (lines); B – the result of OIS and the PM age-depth modeling, with detected hiatuses and their duration (gray rectangles). Arrows show the relation between the hiatuses visible in the profile and the hiatuses detected by the model.

of two independent age-depth models for the parts of the profile below and above the hiatus. This method is commonly used in speleothem science (Lauritzen, 1995; Holzkamper *et al.*, 2005; Vaks *et al.*, 2006; Spötl and Mangini, 2007; Couchoud *et al.*, 2009; Vansteenberghe *et al.*, 2016). The classic age-depth modeling approach on data from the PD-4 stalagmite allows us to estimate the hiatus duration (Fig. 2) as 15.8 ka. It is the time of a break in calcite deposition and possible erosion of the older part of the stalagmite. At this time, caves were flooded a minimum of two times and sand deposition occurred. U-series data of  $19 \pm 0.2$  ka were obtained for samples taken from the thin calcite layer (Fig. 1C) inside the sand, observed only in the axial part of the stalagmite, documenting a short episode of calcite crystallization just after the LGM.

However, in some cases, it is not possible to estimate a reliable age-depth model for continuously deposited parts of the speleothem. First, the quality of the calcite material, for example, strong detrital contamination or extremely low uranium content, may prevent reliable isotope dating results. Second, the studied speleothem age may be beyond the range of the dating method. In such cases, we have limited age information available. Sometimes, obtaining any chronological information is extremely important due to the importance of the paleoenvironmental record preserved in the studied speleothem. The only solutions for obtaining some chronological information are using relative or non-isotopic methods, for example, paleomagnetism, bioindicators, or isotopic stratigraphy. Commonly used paleoclimatic proxies in speleothem science are changes in oxygen isotopic composition. This creates opportunities for using the correlation of the oxygen isotopic record from the studied speleothem with the global/regional reference oxygen curve (OIS approach).

However, the OIS approach presents a few important problems that must be solved. First is the selection of the proper reference curve. The use of marine stack records

such as LR04 is common and reliable when we can assume that the correlated  $\delta^{18}\text{O}$  record reflects over regional changes. Isotopic changes in the studied record and reference curve must be coincident (in the confidence bands of the records) and controlled by the same factors. The main factors shaping the  $\delta^{18}\text{O}$  speleothem records during the last 200 ka in Europe is temperature (Rózański *et al.*, 1993; Moseley *et al.*, 2015; Kern *et al.*, 2019; Comas-Bru *et al.*, 2020) and  $\delta^{18}\text{O}$  composition of precipitation, source effect. The Atlantic Ocean is the main source of moisture for precipitation on the European continent (McDermott *et al.*, 2011). The LR04 is a foraminifera benthic stack record, basing on 57 globally distributed sites. The benthic stack record reflects the variability in  $\delta^{18}\text{O}$  of global nature, and it is driven mostly by changes in the global ice volume. The  $\delta^{18}\text{O}$  speleothem records, driven mostly by source effect and temperature effect, can also reflect long time changes of global nature. Therefore, they can be correlated with LR04 stack record if the global signal is not biased by the influence of regional or local effects. There are differences in the local stacks from Atlantic and Pacific Oceans (Lisiecki and Stern, 2016). The Atlantic regional stacks, which resemble LR04 during MIS 5, display a more gradual transition than the Pacific stacks during glacial–interglacial transitions like MIS 5e/5d. Additionally, there is ca. 0.7 ka bias observed between stack records from Indian and Pacific Oceans. However, majority of the records from LR04 stack (40 sites) is located on Atlantic Ocean (Lisiecki and Raymo, 2005). Therefore, LR04 stack is biased toward Atlantic stack records and is suitable for correlation with European speleothems. When there is more than one potentially available reference curve, running test correlations with all available reference records is recommended, and those that give the better correlation quality indicator are chosen. In the study of RP-66 flowstone from the Reciska Pecina Cave (Hercman *et al.*, submitted) in Slovenia, three

potential reference curves were considered: LR04 (Lisiecki and Raymo, 2005), the stack of oxygen isotope records for Mediterranean Sea sediments (Wang *et al.*, 2010), and the PISO record (Channell *et al.*, 2009). Sixty test correlations were performed for each of those reference curves. The results unambiguously show that the correlations with the MEDI record have the best correlation quality results (Fig. 7) and used for detailed study.

Next, the reference curve and the studied record should be characterized by similar resolution.

Lower resolution causes the loss of recorded information, which makes correlation more difficult. The results of the published tests (Pawlak and Hercman, 2016) show that when the distance between data points becomes larger than the signal period in the record, it causes a large decrease in the correlation quality (Pawlak and Hercman, 2016). The use of OIS for profiles with hiatuses requires a preliminary test of the method used to correlate sensitivity to the lack of part of the record in the correlated profile (breaks in deposition) and how it can influence the normalization procedure, especially if the local extremum is missing in the hiatus part. During initial work with the correlation procedure, we performed a set of tests to determine how the potential hiatus influences the whole correlation procedure, including normalization (Pawlak and Hercman, 2016). The results show that the whole procedure can be robust until the hiatus is no longer than approximately 15% of the whole correlated record length.

The Macedonian stalagmite OH2 (Regattieri *et al.*, 2018) chronology is based on U-series ages (Fig. 8). The U-series ages for this stalagmite have approximately 20 ka large uncertainties, and they are not in proper order (Fig. 8). Therefore, the age-depth models estimated by StalAge (in original paper) and calculated here by MOD-AGE have large error bands. We correlated the  $\delta^{18}\text{O}$  records from this stalagmite with the stack of oxygen isotope records for Mediterranean Sea sediments (MEDI; Wang *et al.*, 2010). From the previous works in a Mediterranean basin, we know that the  $\delta^{18}\text{O}$  records from stalagmites reflect the changes in Mediterranean Sea isotopic composition (Ayalon *et al.*, 2002). The age-depth model obtained by OIS correlation agrees with the age-depth models based on U-series ages. The obtained confidence band varies from ca. 4 to 10 ka. Those differences reflect the quality of correlation for different parts of the correlated records. Intervals with wider confidence bands have larger alignment error, and it reflects the fact that single pick on correlated record can be aligned to reference curve in a different way with similar correlation quality.

The correlation of the older part is reliable, and the shape of the OH2  $\delta^{18}\text{O}$  records agrees with the MEDI record and has a better position than its original chronology (Fig. 8). Therefore, the OIS information potentially

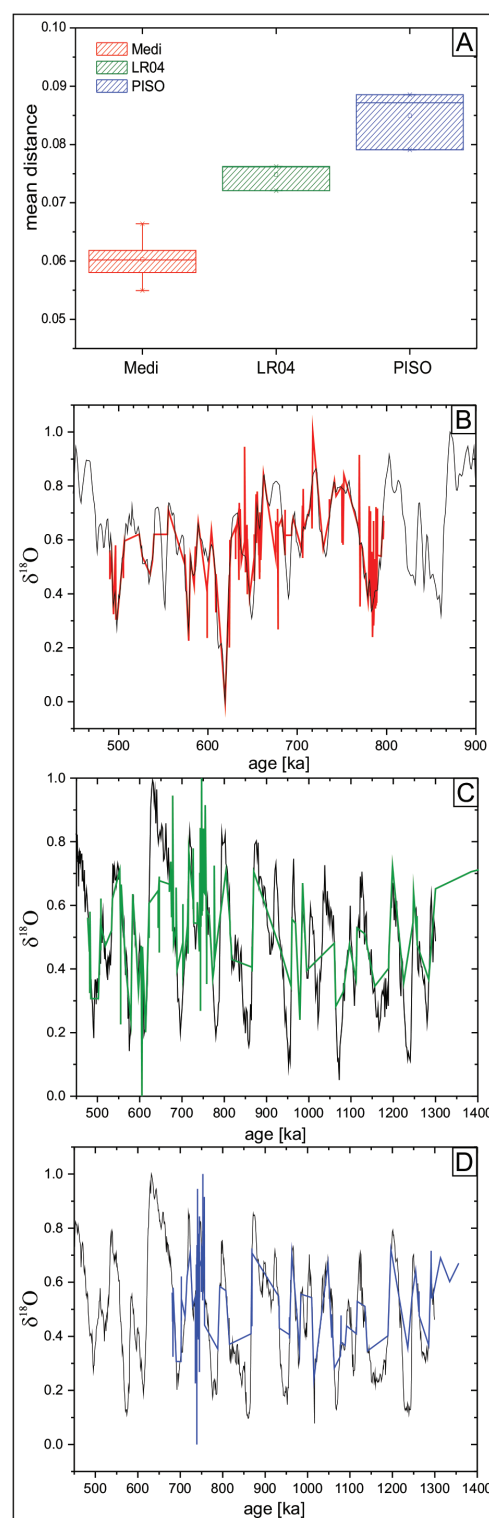


**Fig 7.** The results of testing reference curves: A – quality indicators for the series of test correlations with different reference curves; B – Reciska Pecina curve correlated with the MEDI curve (Wang *et al.* 2010); C – Reciska Pecina curve correlated with the LR04 curve (Lisiecki & Raymo 2005); D – Reciska Pecina curve correlated with the PISO curve (Channell *et al.* 2009).

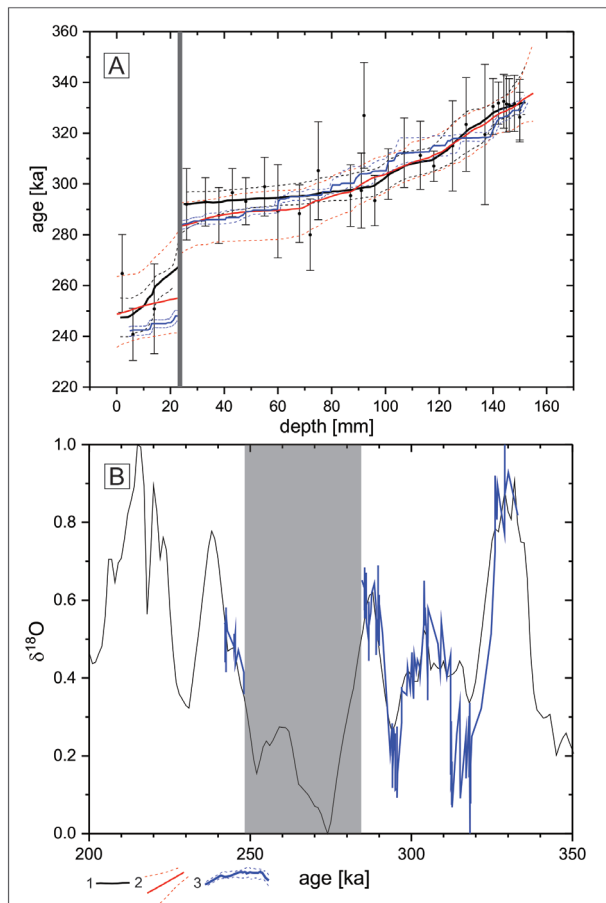


**Fig 8.** The comparison of age-depth models for stalagmites from an unsurveyed Macedonian cave located near Lake Ohrid (Regattieri *et al.* 2018): A – the results of age-depth model estimation – (1) age-depth model made by the authors; (2) age-depth model made by MOD-AGE; (3) age-depth model made by the OIS approach; B – the result of the correlation with the MEDI record (Wang *et al.* 2010).

improves the existing chronology if the assumption about the synchronicity of the records is met. The correlation for the  $\delta^{18}O$  record from the younger part of the stalagmite is more problematic. The GenCorr software correlates only the main trend of the OH2 record here, and the short time pick does not meet its analog on the MEDI curve in this position.

The thin layers located between the two hiatuses may not have enough U-series ages or other independent age benchmarks for age-depth model construction (e.g., Jo *et al.*, 2011, Błaszczuk *et al.*, 2020). In the case of the SC-3 stalagmite, there are three continuous episodes of calcite deposition separated by the two hiatuses. The oldest and the youngest growth phases have sets of reliable U-series ages. Therefore, the classic age-depth modeling approach has been used for the estimation of age borders for the oldest and the youngest crystallization phases (Błaszczuk *et al.*, 2020). The problem is the thin (approximately 10

mm thick) crystallization phase between the hiatuses H1 and H2, where only one reliable U-series age was obtained. The OIS application allows us to estimate the age-depth model between the H1 and H2 hiatuses and estimate their duration as  $7 \pm 6$  and  $13.5^{+11}_{-12}$  ka (Figs. 3 and 4). A similar problem, as described for the SC-3 stalagmite, was identified for the chronology of the stalagmite from Korean Dae-ya Cave (DY-1; Jo *et al.*, 2011). Stalagmite DY-1 contains three growth phases (A, B, and C), separated by the two hiatuses (Fig. 9). The 5-mm-thick phase B is located between the two hiatuses, and its age is documented by only one U-series age. Therefore, the authors were not able to estimate a robust age-depth model for this phase based on the classic age-depth modeling approach. The authors estimate the mean growth rate for phase B based on the U-series ages below and above the hiatus ( $0.5 \text{ mm.k}^{-1}$ ). In fact, the estimate assumes the duration of the hiatus is approximately 0 ka. The published record of  $\delta^{18}O$  from DY-1 has been presented only on a depth scale (Jo *et al.*, 2011). Here, for DY-1 data, we used the same OIS approach as that in the case of the SC-3 stalagmite (Fig. 9). The  $\delta^{18}O$  record from phase B of the DY-1 stalagmite can be correlated well with the MIS 5e/5d transition time (Fig. 8A). Additionally, it is in agreement with the published U-series age (Fig. 8B). Based on the added chronological information, the duration of the younger hiatus can be estimated as  $97.5^{+0.8}_{-0.5}$  ka. The duration of the older hiatus was rather short, probably less than 1 ka. Based on our approach, the mean growth rate for phase B was between  $0.3$  and  $0.5 \text{ mm.k}^{-1}$ . Using the proposed approach allows us to estimate the chronology for the full profile of the studied stalagmite.

There are many stalagmites, where the chronology error is not well defined (Comas-Bru *et al.*, 2020). For example, the authors do not provide the continuous confidence bands for their chronology of the speleothem from Spanish Cobre Cave. Its chronology is based on the sets of U-series samples and fluorescence lamina counting (Fl). They only stated that the  $2 \sigma$  error of the estimated age-depth model is 1.5 ka, and it includes the U-series age error; the potential error of Fl is not included. This speleothem has three growing phases divided by two principal hiatuses (Rossi *et al.*, 2014). The age difference between the dated points counted by the Fl is in good agreement with the U-series ages (Fig. 10; black line). The main problem with this dataset is the low number of U-series ages for the youngest growing phase (Ph3) and their large uncertainties of more than 3.5 ka (Fig. 10). Even, if estimated by Fl, age-depth model fits the U-series age well. The age-depth model here should be considered as less reliable. The MOD-AGE software requires at least three dated points for age-depth model calculation. Therefore, we used MOD-AGE here only to estimate the age-depth model for the Ph1 and Ph2 phases (Fig. 10). The age-depth models estimated by MOD-AGE are generally smoother than the

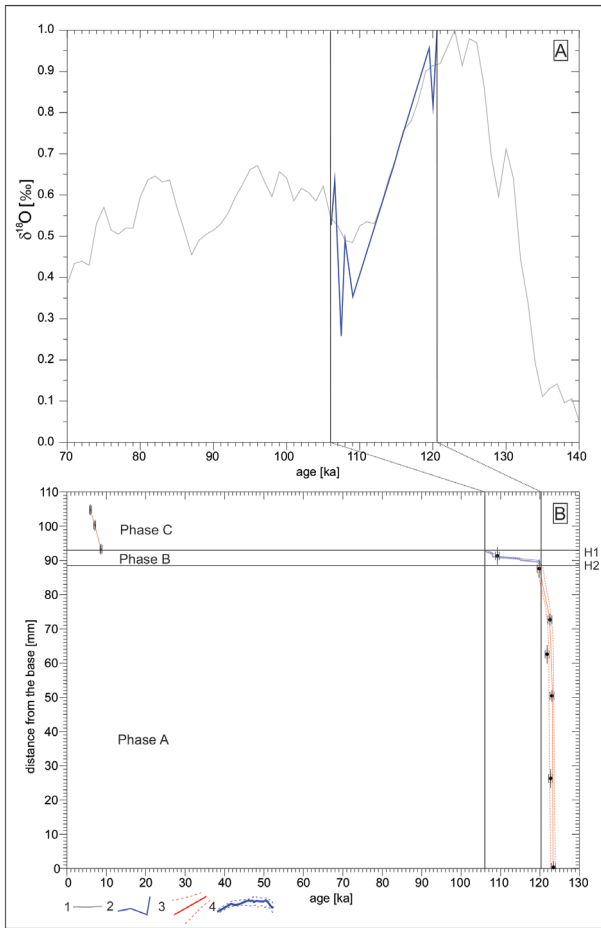


**Fig 9.** The result of correlation of the DY-1  $\delta^{18}\text{O}$  record with the LR04 record: A – the  $\delta^{18}\text{O}$  record correlated with LR04; B – age-depth model estimated for phase B (blue lines) and age-depth models estimated for phases A and C based on the U-series ages (data from Jo *et al.* 2011) – (1) LR04 record; (2) DY-1  $\delta^{18}\text{O}$  record; (3) age-depth model made by the authors (Jo *et al.* 2011); (4) age-depth model made by the OIS approach.

FI models. However, the FI models are in good agreement with the MOD-AGE models (Fig. 10; black lines and red lines). The OIS approach was used here as a third method for estimating the durations of hiatuses. The  $\delta^{18}\text{O}$  recorded in stalagmites from Cobra Cave is under the strong influence of moisture from Atlantic sources (Rossi *et al.*, 2014). Therefore, we chose the GRIP record as the reference record. The GRIP chronology bases on ice flow and snow accumulation model “ss09sea” (Johnsen *et al.*, 2001). To check potential diachronicity with speleothem records, the Greenland ice core record can be compared with Hulu Cave stalagmite (Lisiecki and Stern 2016). The comparison by matching the onset of interstadials on both records shows differences up to 0.8 ka (Lisiecki & Stern 2016). Observed chronological bias is lower than the large uncertainty of U-series ages measured in the stalagmite from Cobra Cave (Rossi *et al.*, 2014). Therefore, in this specific case, correlation with the GRIP record can bring additional chronological information. The

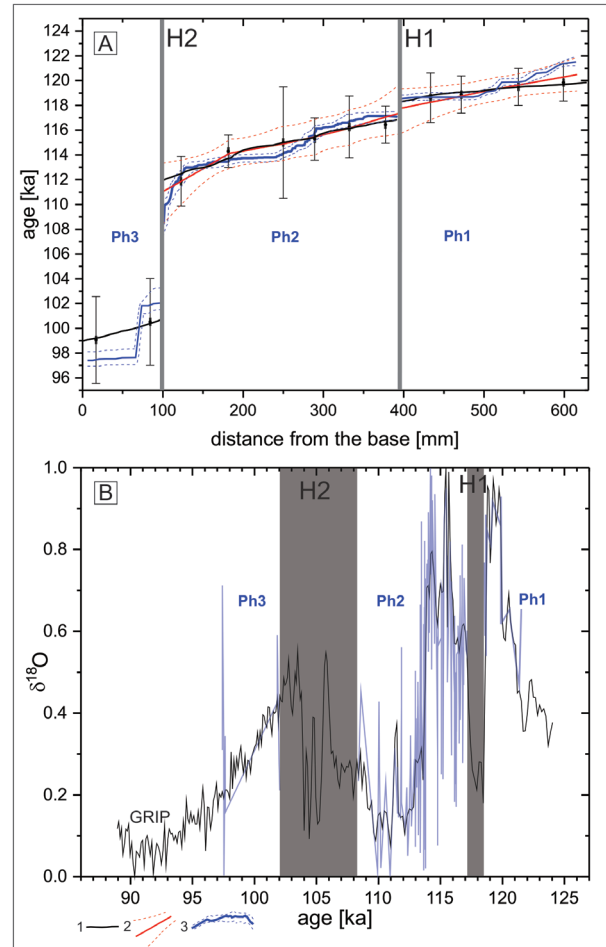


**Fig 10.** The comparison of age-depth models for stalagmites from Spanish Cobra Cave (Rossi *et al.* 2014): A – the results of age-depth model estimation – (1) age-depth model made by the authors, fluorescence lamina counting (FI); (2) age-depth model made by MOD-AGE; (3) age-depth model made by the OIS approach; B – the result of the correlation with the GRIP record.

results of the performed correlation are in agreement with the age-depth model estimated by MOD-AGE (Fig. 10A; red and blue lines). During the hiatus (H1), the GRIP record has strong events of low values, which increases the reliability of this correlation (Fig. 10B). The age-depth model estimated by the OIS approach is sharper than the FI model. However, for the Ph1 and Ph2 phases, it is in good agreement with the FI model. In the case of the Ph3 phase, both models are in agreement with two U-series ages. However, the age-depth model estimated by the OIS approach suggests additional growth cessation between 102 and 98 ka. The model estimated by FI is more regular (Fig. 10A). However, due to large errors of U-series ages for Ph3, its reliability is low. Additionally, the correlation of the  $\delta^{18}\text{O}$  record from Ph3 with the GRIP record is not reliable. The GenCorr software is not able to find positions with a sufficiently low mean distance between the correlated records. At that time,

local factors had a stronger influence on  $\delta^{18}\text{O}$ . Therefore, its shape does not reflect regional and global changes well and cannot be used as alternative age-depth model.

In the previous examples, we used U-series ages as the pointed age benchmarks, and every depositional episode had at least one defined age benchmark. The last example (LDH profile) is beyond the U-series age limits. Additionally, the uranium concentrations measured in a set of samples from this profile are lower than 0.07 ppm (Häuselmann *et al.*, 2015). It is far too low for eventual application of U–Pb dating. The LDH profile chronology is based on eight paleomagnetic benchmarks (Table 2). The whole profile has ten principal hiatuses and eleven sedimentation phases. Therefore, the number of points with defined ages is far too low to estimate age-depth models for the individual sedimentation phases. In this case, due to the LDH profile age and its duration, the LR04 stack record is the only robust  $\delta^{18}\text{O}$  record available that covers the required interval.

One of the advantages of GenCorr software is the sensitivity for deposition breaks (see Pawlak & Hercman 2016). The OIS+PM chronology may be verified by comparisons of the locations of hiatuses derived from the correlation results with their actual positions in the LDH section (Fig. 6A). The whole LDH profile is correlated to the LR04 record with no assumption about continued/discontinued deposition (Fig. 5; black line). The OIS+PM age-depth model suggests nine hiatuses, all of which can be identified with breaks in the LDH lithological log (arrows between panels A and B in Fig. 6). However, within the LDH speleothem profile, the accuracy of the OIS chronology will

depend primarily on the precision of the field measurements of PM sample position. These were mostly within 1–2 cm, with a maximum of 4 cm (Table 2). In general, we may state that unconformities/hiatuses detected by the combined OIS+PM chronology are in relatively good agreement with the lithological log.

A comparison of the ages estimated for the LDH with the GPTS records (Ogg 2012) shows that hiatuses can significantly distort magnetozone stratigraphic relationships, especially their thicknesses. This effect is particularly strong for zones N2 and N3 in the younger part of the LDH profile and for zones N6 and R6 in the older segments. The duration of breaks in deposition is much longer than that suggested by Bosák *et al.*, (2002). The longest periods of non-deposition are detected inside the N3, R2, and R3 zones and cover time spans of approximately 185, 100 and 95 ka, respectively (Fig. 11).

## 6. Conclusions

Deposition breaks in speleothems are often caused by climatic factors, so they are carriers of climatic information. Hence, the correct and possibly accurate estimation of the durations of breaks is important for accurate paleoclimatic reconstructions.

The approach based on two dated points located close to hiatus boundaries may not be precise enough to estimate the time hidden in the hiatus because dated points are never located directly on the hiatus boundaries. The age-depth modeling approach gives robust results. However, it is not

**Table 2.** Position of magnetozones in the LDH profile.

Age* [Ma]	Polarity chron*	Magneto- zone	Paleomagnetic benchmarks		
			Symbol	Depth** [cm]	Age*** [Ma]
(2.581–) <3.03	C2An.1n	N1			
			N1/R1	13 ± 4	3.03 ± 0.03
3.03–3.12	C2An.1r	R1	R1/N2	32 ± 1	3.12 ± 0.03
3.12–3.21	C2An.2n	N2	N2/R2	39 ± 2	3.21 ± 0.035
3.21–3.33	C2An.2r	R2	R2/N3	53 ± 2	3.33 ± 0.035
3.33–3.60	C2An.3n	N3	N3/R3	60 ± 1	3.60 ± 0.04
3.60–4.19	C2Ar	R3	R3/N4	124 ± 1	4.19 ± 0.04
4.19–4.30	C3n.1n	N4	N4/R4	139 ± 2	4.30 ± 0.045
4.30–4.49	C3n.1r	R4	R4/N5	151 ± 4	4.49 ± 0.045
4.49–4.63	C3n.2n	N5	N5/R5	167 ± 2	4.63 ± 0.05
4.63–4.80	C3n.2r	R5	R5/N6	195 ± 2	4.80 ± 0.05
4.80–4.90	C3n.3n	N6	N6/R6	200 ± 1	4.90 ± 0.05
4.90–4.98	C3n.3r	R6	R6/N7	218 ± 1	4.98 ± 0.05
>4.98(–5.23)	C3n.4n	N7			

Explanations: N – normal polarity, R – reverse polarity; \*after Ogg (2012); \*\* depth with error; \*\*\* age with assumed age uncertainty (for explanations, see the text). PM benchmarks marked as *italic* are located at hiatuses and were not included into PM+OIS chronology.

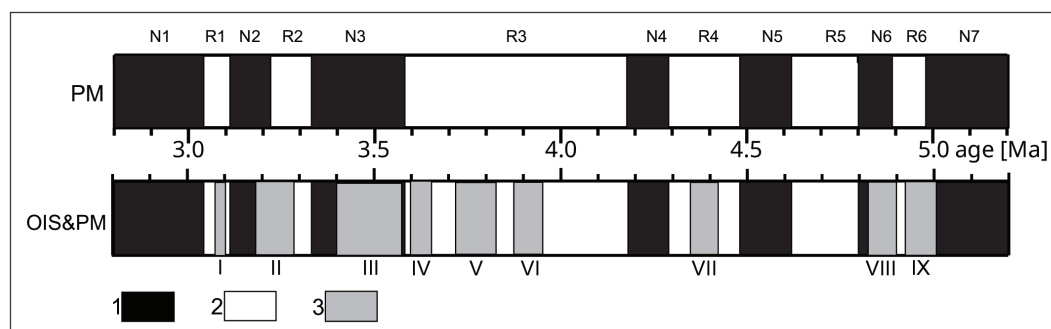


**Fig 11.** The comparison of the GPTS record (Ogg 2012) with the time scale of the LDH section obtained by integrated OIS and PM chronology: 1 – normal polarity, 2 – reverse polarity, 3 – non-deposition time (hiatus).

always possible to have a sufficient number of age data to calculate independent age-depth models for individual depositional phases.

Our study shows different situations in several examples of speleothems with hiatuses: (1) stalagmite PD-4 (Slovakia), where the hiatus duration was estimated by the classic age-depth modeling approach based only on U-series data; (2) stalagmite SC-3 (Poland), where oxygen isotopic stratigraphy is used to establish the chronology in a part of the stalagmite with only one U-series age; and (3) the flowstone profile from Ledena Dvorana in Slovenia, where the chronology bases on paleomagnetic benchmarks and oxygen isotopic stratigraphy. Additionally, the three examples selected from the literature: (1) a stalagmite from Daeya Cave (Korea); (2) a stalagmite from Cobre Cave (Spain); and (3) one stalagmite from a Macedonian cave located near Lake Ohrid, were used. In the case of two examples, first from Cobra Cave and second from the Macedonian cave, the long  $\delta^{18}\text{O}$  record can have episodes when local conditions have a strong impact on its values, and this part of that record cannot be correlated to the reference curve. Therefore, the results of the OIS correlation should be verified by independent chronology, such as U-series ages. Nevertheless, the OIS approach combined with the independent chronological information, such as U-series ages, can be helpful for the detection of hiatuses and estimation of their duration. Finally, the flowstone profile of the Ledena Dvorana (LDH;

Slovenia)-layered complex, divided by ten principal hiatuses, is an example of a profile where the OIS approach is the only reliable option for determining the chronology of all deposition phases. The obtained OIS age-depth model is in accordance with PM benchmarks and with hiatuses detected in the profile. Generally, the OIS correlation can be a useful tool for the estimation of duration of hiatuses and chronology of the speleothem profiles beyond the U-series age limits. Additionally, the OIS approach can be used for the improvement of the existing chronologies with a large error. The main threats for this approach are potential diachronicity of the reference curve and correlated record.

## Acknowledgements

Analyses of SC-3 sample were supported by the National Science Centre, Poland, Grant No. 2016/23/N/ST10/00067. Stable isotope analyses and the OIS approach were funded by the Institute of Geological Sciences PAS as the “OIS” and “HIATUSY” internal projects.

Research was supported by the bilateral mobility cooperation nos. SAZU-16-03, SAZU-19-01, and PAN-17-22 by the Plan of the Institutional Financing of the Institute of Geology of the Czech Academy of Sciences (No. RVO67985831), by the Slovenian Research Agency (research core funding Nos. P6-0119 and P6-0618, and by research project nos. J6-3035-0618-01 and J6-6345-0618-04).

## References

- Ayalon, A, Bar-Matthews, M, and Kaufman, A, 2002. Climatic conditions during marine oxygen isotope stage 6 in the eastern Mediterranean region from the isotopic composition of speleothems of Soreq Cave, Israel. *Geology* 30: 303.
- Andersen KK, Azuma N, Barnola JM, Bigler M, Biscaye P, Cailion N, Chappellaz J, Clausen HB, Dahl-Jensen D, Fischer H, Fluckiger J, Fritzsche D, Fujii Y, Goto-Azuma K, Grønvald K, Gundestrup NS, Hansson M, Huber C, Hvidberg CS, Johnsen SJ, Jonsell U, Jouzel J, Kipfstuhl S, Landais A, Leuenberger M, Lorrain R, Masson-Delmotte V, Miller H, Motoyama H, Narita H, Popp T, Rasmussen SO, Raynaud D, Rothlisberger R, Ruth U, Samyn D, Schwander J, Shoji H, Siggard-Andersen ML, Steffensen JP, Stocker T, Sveinbjörnsdóttir AE, Svensson A, Takata M, Tison JL, Thorsteinsson Th, Watanabe O, Wilhelms F, and White JWC, 2004. High-resolution record of Northern Hemisphere climate extending into the last interglacial period. *Nature* 431-7005: 147-151, DOI: [10013/epic.20716](https://doi.org/10.1038/epic.20716).

- Baker A, Smart PL, Ford DC, 1993. Northwest European palaeoclimate as indicated by growth frequency variation of secondary calcite deposits. *Palaeogeography, Palaeoclimatology, Palaeoecology* 100: 291-301, DOI: [10.1016/0031-0182\(93\)90059-R](https://doi.org/10.1016/0031-0182(93)90059-R).
- Banner JL, Guilfoyle A, James EW, Stern LA, and Musgrove ML, 2007. Seasonal Variations in Modern Speleothem Calcite Growth in Central Texas, U.S.A. *Journal of Sedimentary Research* 77 (8): 615–622, DOI: [10.2110/jsr.2007.065](https://doi.org/10.2110/jsr.2007.065).
- Błaszczak M, Hercman H, Pawlak J, and Szczygiał J, 2020. Paleoclimatic reconstruction in the Tatra Mountains of the western Carpathians during MIS 9–7 inferred from a multiproxy speleothem record. *Quaternary Research* – accepted, 10.1017/qua.2020.69.
- Boch R, Cheng H, Spötl C, Edwards RL, Wang X, and Häuselmann Ph, 2011. NALPS: a precisely dated European climate record 120–60 ka. *Climate of the Past* 7: 1247 – 2011, DOI: [10.5194/cp-7-1247-2011](https://doi.org/10.5194/cp-7-1247-2011).
- Bosák P, Hercman H, Mihevc A and Pruner P, 2002. High resolution magnetostratigraphy of speleothems from Snežna Jama, Kamniške-Savinja Alps, Slovenia. *Acta Carsologica* 31: 15–32, DOI: [10.3986/ac.v31i3.377](https://doi.org/10.3986/ac.v31i3.377).
- Borówka RK, Kostrzewski A, and Zwolinski Z, 1985. Cave sediments from the Chochołowska Valley (the Tatra Mountains, Poland); interpretation of sequences and depositional processes. *Quaestiones Geographicae*: 5-24.
- Channell, JET, Xuan, C, and Hodell, DA, 2009. Stacking paleointensity and oxygen isotope data for the last 1.5 Myr (PISO-1500). *Earth Planet. Sci. Lett.* 283: 14–2, DOI: [10.1016/j.epsl.2009.03.012](https://doi.org/10.1016/j.epsl.2009.03.012).
- Cheng H, Edwards RL, Shen CC, Polyak VJ, Asmerom Y, Woodhead J, Hellstrom J, Wang Y, Kong X, Spötl C, Wang X and Alexander EC, 2013. Improvements in <sup>230</sup>Th dating, <sup>230</sup>Th and <sup>234</sup>U half-life values, and U-Th isotopic measurements by multi-collector inductively coupled plasma mass spectrometry. *Earth and Planetary Science Letters* 371–372: 82–91, DOI: [10.1016/j.epsl.2013.04.006](https://doi.org/10.1016/j.epsl.2013.04.006).
- Comas-Bru, L, Rehfeld, K, Roesch, C, Amirnezhad-Mozhdehi, S, Harrison, SP, Atsawawaranunt, K, Ahmad, SM, Ait Brahim, Y, Baker, A, Bosomworth, M, Breitenbach, SFM, Burstyn, Y, Columbu, A, Deininger, M, Demény, A, Dixon, B, Fohlmeister, J, Hatvani, IG, Hu, J, Kaushal, N, Kern, Z, Labuhn, I, Lechleitner, FA, Lorrey, A, Martrat, B, Novello, VF, Oster, J, Pérez-Mejías, C, Scholz, D, Scroxton, N, Sinha, N, Ward, BM, Warken, S, Zhang, H, and the SISAL members: SISALv2 2020: A comprehensive speleothem isotope database with multiple age-depth models, *Earth Syst. Sci. Data Discuss.*, in review.
- Couchoud I, Genty D, Hoffmann, D, Drysdale R and Blamart D, 2009. Millennial-scale climate variability during the Last Interglacial recorded in a speleothem from south-western France. *Quat. Sci. Rev.* 28: 3263–3274, DOI: [10.1016/j.quascirev.2009.08.014](https://doi.org/10.1016/j.quascirev.2009.08.014).
- Fairchild IJ and Baker A, 2012. *Speleothem Science. From Process to Past Environments*. Oxford John Wiley and Sons, 416 pp.
- Fankhauser A, McDermott F and Fleitmann D, 2016. Episodic speleothem deposition tracks the terrestrial impact of millennial-scale last glacial climate variability in SW Ireland. *Quat. Sci. Rev.* 152: 104–117, DOI: [10.1016/j.quascirev.2016.09.019](https://doi.org/10.1016/j.quascirev.2016.09.019).
- Fisher R, 1953. Dispersion on a sphere. *Proc. R. Soc. Lond.* 217: 295–305. DOI: [10.1098/rspa.1953.0064](https://doi.org/10.1098/rspa.1953.0064).
- Frisia, S, Borsato, A, Preto, N, and McDermott, F, 2003. Late Holocene annual growth in three Alpine stalagmites record the influence of solar activity and the North Atlantic oscillation on winter climate. *Earth and Planetary Science Letters* 216: 231-439, DOI: [10.1016/S0012-821X\(03\)00515-6](https://doi.org/10.1016/S0012-821X(03)00515-6).
- Hellstrom J, 2003. Rapid and accurate U/Th dating using parallel ion-counting multicollector ICP-MS. *J. Anal. At. Spectrom.* 18: 135–1346, DOI: [10.1039/B308781F](https://doi.org/10.1039/B308781F).
- Hercman H, Nowicki T and Lauritzen SE, 1998. Development of Szczelina Chochołowska cave (Western Tatra Mts.), based on uranium-series dating of speleothems. *Studia Geologica Polonica* 113: 85–103.
- Hercman H and Pawlak J, 2012. MOD-AGE: An age-depth model construction algorithm. *Quaternary Geochronology* 12: 1–10, DOI: [10.1016/j.quageo.2012.05.003](https://doi.org/10.1016/j.quageo.2012.05.003).
- Herich P, 2017. Demänová caves. The most extensive underground karst phenomenon in Slovakia. *Bulletin of the Slovak Speleological Society*: 27–38.
- Holden EN, 1990. Total half-lives for selected nuclides. *Pure and Applied Chemistry* 62: 941–958, DOI: [10.1351/pac199062050941](https://doi.org/10.1351/pac199062050941).
- Holzhammer S, Mangini, A, Spötl, C, Mudelsee, M, 2004. Timing and progression of the Last Interglacial derived from a high alpine stalagmite. *Geophysical Research Letter* 31, L07201. DOI: [10.1029/2003GL019112](https://doi.org/10.1029/2003GL019112).
- Holzhammer S, Spötl C and Mangini A, 2005. High-precision constraints on timing of Alpine warm periods during the middle to late Pleistocene using speleothem growth periods. *Earth Planet. Sci. Lett.* 236: 751–764, DOI: [10.1016/j.epsl.2005.06.002](https://doi.org/10.1016/j.epsl.2005.06.002).
- Hu C, Henderson GM, Huang J, Xie S, Sun Y, and Johnson KR, 2008. Quantification of Holocene Asian monsoon rainfall from spatially separated cave records. *Earth and Planetary Science Letters* 266: 221-232, DOI: [10.1016/j.epsl.2007.10.015](https://doi.org/10.1016/j.epsl.2007.10.015).
- Ivanovich M and Harmon RS, 1992. *Uranium Series Disequilibrium. Applications to Earth, Marine, and Environmental Sciences.*, Oxford, Oxford Science Publications: 910 pp.
- Jaffey AH, Flynn KF, Glendenin LE, Bentley WC and Essling AM, 1971. Precision measurement of half-lives and specific activities of <sup>235</sup>U and <sup>238</sup>U. *Physical Review C4*: 1889–1906, DOI: [10.1103/PhysRevC.4.1889](https://doi.org/10.1103/PhysRevC.4.1889).
- Jelínek V, 1966. A high sensitivity spinner magnetometer. *Stud. Geophys. Geod.* 10: 58–78, DOI: [10.1007/BF02590052](https://doi.org/10.1007/BF02590052).

- Jelínek V, 1973. Precision A.C. bridge set for measuring magnetic susceptibility and its anisotropy. *Stud. Geophys. Geod.* 17: 36–48, DOI: [10.1007/BF01614027](https://doi.org/10.1007/BF01614027).
- Jo KN, Woo KS, Lim HS, Cheng H, Edwards RL, Wang Y, Jiang X, Kim R, Lee JI, Yoon HI and Yoo KC, 2011. Holocene and Eemian climatic optima in the Korean Peninsula based on textural and carbon isotopic records from the stalagmite of the Daeya Cave, South Korea. *Quat. Sci. Rev.* 30: 1218–1231, DOI: [10.1016/j.quascirev.2011.02.012](https://doi.org/10.1016/j.quascirev.2011.02.012).
- Johnsen SJ, Dahl-Jensen D, Gundestrup N, Steffensen JP, Clausen HB, Miller H, Masson-Delmotte V, Sveinbjörnsdóttir AE, White J, 2001. Oxygen isotope and palaeotemperature records from six Greenland ice-core stations: Camp Century, Dye-3, GRIP, GISP2, Renland, and NorthGRIP. *J. Quat. Sci.*, 16, 299–307, DOI: [10.1002/jqs.622](https://doi.org/10.1002/jqs.622).
- Kern Z, Demény A, Perşoiu A, and Hatvani IG, 2019. Speleothem Records from the Eastern Part of Europe and Turkey—Discussion on Stable Oxygen and Carbon Isotopes. *Quaternary* 2: 3–31.
- Kirschvink JL, 1980. The least-squares line and plane and the analysis of palaeomagnetic data. *Geoph. J. Royal Astronom. Soc.* 62: 699–718, DOI: [10.1111/j.1365-246X.1980.tb02601.x](https://doi.org/10.1111/j.1365-246X.1980.tb02601.x).
- Lauritzen SE, 1995: High-resolution paleotemperature proxy record during the last interglaciation in Norway from speleothems. *Quaternary Research* 43: 133–46, DOI: [10.1006/qres.1995.1015](https://doi.org/10.1006/qres.1995.1015).
- Lisiecki LE and Raymo ME, 2005. A Pliocene-Pleistocene stack of 57 globally distributed benthic  $\delta^{18}\text{O}$  records, *Paleoceanography* 20: PA1003, DOI: [10.1029/2004PA001071](https://doi.org/10.1029/2004PA001071).
- Lisiecki LE and Stern JV, 2016. Regional and global benthic  $\delta^{18}\text{O}$  stacks for the last glacial cycle, *Paleoceanography*, 31: 1368–1394, DOI: [10.1002/2016PA003002](https://doi.org/10.1002/2016PA003002).
- McDermott F, Atkinson TC, Fairchild IJ, Baldini LM, and Matthey DP, 2011. A first evaluation of the spatial gradients in  $\delta^{18}\text{O}$  recorded by European Holocene speleothems. *Global and Planetary Change*, 79: 275–287.
- Meyer, MC, Spötl, C, and Mangini, A, 2008. The demise of the Last Interglacial recorded in isotopically dated speleothems from the Alps. *Quaternary Science Reviews* 27: 476–496, DOI: [10.1016/j.quascirev.2007.11.005](https://doi.org/10.1016/j.quascirev.2007.11.005).
- Moseley, GE, Spötl, C, Cheng, H, Boch, R, Min, A, Edwards, LR, 2015. Termination-II interstadial/stadial climate change recorded in two stalagmites from the north European Alps. *Quaternary Science Reviews* 127: 229–239. DOI: [10.1016/j.quascirev.2015.07.012](https://doi.org/10.1016/j.quascirev.2015.07.012).
- Moseley, GE, Spötl, C, Brandstätter, S, Erhardt, T, Luetscher, M, and Edwards, RL, 2020. NALPS19: sub-orbital-scale climate variability recorded in northern Alpine speleothems during the last glacial period, *Clim. Past*, 16: 29–50, DOI: [10.5194/cp-16-29-2020](https://doi.org/10.5194/cp-16-29-2020).
- Mioć P and Žnidarčič M, 1983. *Osnovna geološka karta SFRJ (Geological map of SFRJ), list Ravne na Koroškem, 1 : 100 000*. Beograd, Zvezni geološki zavod.
- Nowicki T, 1996. *Geologia jaskini Szczelina Chochołowska, Wyżnia Brama Chochołowska, Tatry Zachodnie. (Geology of Szczelina Chochołowska Cave, Wyżnia Brama Chochołowska, Western Tatra Mts.)*. *Przyroda TPN a Człowiek, t. I*, Kraków-Zakopane: 102–104. (In Polish).
- Ogg JG, 2012. Geomagnetic polarity time scale. In: Gradstein F.M., Ogg J.G., Schmitz M., eds. *The Geologic Time Scale*. Amsterdam, Elsevier: 85–113.
- Pawlak J and Hercman H, 2016. Numerical correlation of speleothem stable isotope records using a genetic algorithm. *Quaternary Geochronology* 33: 1–12, DOI: [10.1016/j.qua-geo.2015.12.005](https://doi.org/10.1016/j.qua-geo.2015.12.005).
- Příhoda K, Krs M, Pešina B and Bláha J, 1989. MAVACS - a new system of creating a non-magnetic environment for palaeomagnetic studies. *Cuad. Geol. Ibér.* 12: 223–250.
- Roberts, MS, Smart, PL, Baker, A, 1998. Annual trace element variations in a Holocene speleothem. *Earth Planetary Science Letters* 154: 237–246.
- Rossi C, Mertz-Kraus R, Osete MR 2014, Paleoclimate variability during the Blake geomagnetic excursion (MIS 5d) deduced from a speleothem record, *Quaternary Science Reviews*, 102: 166–180.
- Sadler PM, 1981. Sediment accumulation rates and the completeness of stratigraphic sections. *J. Geol.* 89: 569–584.
- Spötl C and Mangini A, 2007. Speleothems and paleoglaciers. *Earth Planet. Sci. Lett.* 254: 323–331, DOI: [10.1016/j.epsl.2006.11.041](https://doi.org/10.1016/j.epsl.2006.11.041).
- Steponaitis E, Andrews A, McGee D, Quade J, Hsieh YT, Broecker WS, Shuman BN, Burns SJ and Cheng H, 2015. Mid-Holocene drying of the U.S. Great Basin recorded in Nevada speleothems. *Quaternary Science Reviews* 127: 174–185, DOI: [10.1016/j.quascirev.2015.04.011](https://doi.org/10.1016/j.quascirev.2015.04.011).
- Vaks A, Bar-Matthews M, Ayalon A, Matthews A, Frumkin A, Dayan U, Halicz L, Almogi-Labin A and Schilman B, 2006. Paleoclimate and location of the border between Mediterranean climate region and the Saharo-Arabian Desert as revealed by speleothems from the northern Negev Desert, Israel. *Earth Planet. Sci. Lett.* 249: 384–399, DOI: [10.1016/j.epsl.2006.07.009](https://doi.org/10.1016/j.epsl.2006.07.009).
- Vansteenberghe S, Verheyden S, Cheng H, Edwards RL, Keppens E and Claeys P, 2016. Paleoclimate in continental northwestern Europe during the Eemian and early Weichselian (125–97 ka): insights from a Belgian speleothem. *Clim. Past* 12: 1445–1458, DOI: [10.5194/cp-12-1445-2016](https://doi.org/10.5194/cp-12-1445-2016).
- Wang YJ, Cheng H, Edwards RL, An ZS, Wu JY, Shen CC, and Dorale JA, 2001. A high-resolution absolute-dated Late Pleistocene monsoon record from Hulu cave, China. *Science* 294: 2345–2348, DOI: [10.1126/science.1064618](https://doi.org/10.1126/science.1064618).
- Wang YJ, Cheng H, Edwards RL, He Y, Kong X, An Z, Wu J, Kelly MJ, Dykoski CA, Li X, 2005. The Holocene Asian monsoon: links to solar changes and North Atlantic climate. *Science* 308: 854, DOI: [10.1126/science.1106296](https://doi.org/10.1126/science.1106296).

Wang, P, Tian, J, Lourens, LJ, 2010. Stack of stable carbon and oxygen isotope record for 733 Mediterranean Sea sediments. *Earth and Planetary Science Letters* 290: 319, 330

Yuan D, Cheng H, Edwards RL, Dykoski CA, Kelly MJ, Zhang M, Qing J, Lin Y, Wang Y, Wu J, Dorale JA, An Z, Cai Y, 2004.

Timing, duration, and transitions of the last Interglacial Asian monsoon. *Science* 304, 575-578, DOI: [10.1126/science.1091220](https://doi.org/10.1126/science.1091220).

Zupan Hajna N, Mihevc A, Pruner P and Bosák P, 2008. Palaeomagnetism and Magnetostratigraphy of Karst Sediments in Slovenia. *Carsologica*, 8, Založba ZRC, Ljubljana: 266 pp.